frontiers in Earth Science

ORIGINAL RESEARCH
published: 19 July 2021
doi: 10.3389/feart.2021.689087

Strain Transformation Adjacent to the West Qinling Orogen: Implications for the Growth of the Northeastern Tibetan Plateau

Zhangjun Li[1,2]*, *Feng Cheng*[3,4], *Ming Hao*[1]*, *Zachary M. Young*[5], *Shangwu Song*[1], *Fan Yang*[1] *and Wenquan Zhuang*[1]

[1]The Second Monitoring and Application Center, China Earthquake Administration, Xi'an, China, [2]State Key Laboratory of Earthquake Dynamics, Institute of Geology, China Earthquake Administration, Beijing, China, [3]Key Laboratory of Orogenic Belts and Crustal Evolution, School of Earth and Space Sciences, Ministry of Education, Peking University, Beijing, China, [4]Nevada Bureau of Mines and Geology, University of Nevada, Reno, NV, United States, [5]Nevada Geodetic Laboratory, University of Nevada, Reno, NV, United States

OPEN ACCESS

Edited by:
David K. Wright,
University of Oslo, Norway

Reviewed by:
Xiaoyu Guo,
Sun Yat-Sen University, China
Lupeng Zhang,
The Ohio State University, United States

***Correspondence:**
Zhangjun Li
george_jun@hotmail.com
Ming Hao
ha_mg@163.com

Specialty section:
This article was submitted to Quaternary Science, Geomorphology and Paleoenvironment, a section of the journal Frontiers in Earth Science

Received: 31 March 2021
Accepted: 02 July 2021
Published: 19 July 2021

Citation:
Li Z, Cheng F, Hao M, Young ZM, Song S, Yang F and Zhuang W (2021) Strain Transformation Adjacent to the West Qinling Orogen: Implications for the Growth of the Northeastern Tibetan Plateau. Front. Earth Sci. 9:689087. doi: 10.3389/feart.2021.689087

The West Qinling orogen has played an important role in accommodating the deformation in the northeastern Tibetan Plateau induced by the India-Eurasia convergence. Here we construct a vertical land motion (VLM) model based on the latest leveling observations adjacent to the West Qinling orogen. Combined with the horizontal deformation field, the crustal deformation pattern in this area is investigated. Additionally, slip rate and coupling coefficients of the West Qinling fault, the longest fault separating the West Qinling orogen from the Lanzhou (Longxi) block, are inverted and constrained with GPS and VLM observations. Results show that the West Qinling fault slips slowly at a rate of 1–2 mm/yr and is strongly coupled with a moment magnitude deficit of *Mw*7.4. The crustal uplift rates adjacent to the West Qinling orogen are 0–3 mm/yr; which combined with 0–12.5 × 10^{-9}/yr contraction rates, suggests that strain transformation plays a key role in controlling the tectonic uplift in the West Qinling orogen, and furthers our understanding of the contemporary geomorphic and topographic features. We identify a significant deformation transition belt at longitudes of 105°–106°E, which indicates that crustal deformation, induced from the northeastern expansion of the Tibetan Plateau, is mainly constrained to the plateau, rather than accommodated by crustal materials escaping eastward along the Qinling Mountains.

Keywords: the west qinling orogen, strain transformation, vertical land motion, leveling observations, moment deficit

HIGHLIGHTS

1. A vertical land motion model adjacent to the West Qinling orogen is constructed based on leveling observations.
2. Strain transformation plays an important role in controlling the tectonic uplift in the West Qinling orogen.
3. The West Qinling fault has a moment magnitude accumulation of *Mw*7.4, and thus exhibits high seismic risk.

INTRODUCTION

Strain patterns adjacent to convergent plate boundaries, especially along continent-continent collision zones such as the Tibetan Plateau and Anatolian Plateau, remains a source of active investigation (England et al., 1985; Tapponnier, 2001; Reilinger et al., 2006). Known as the "roof of the world," the Tibetan Plateau is famous for its high average elevation of 4,000 m, as well as complex tectonics and deformation patterns those are driven by the India-Eurasia convergence (Molnar & Tapponnier, 1975; Tapponnier et al., 1982; Tapponnier, 2001). Horizontal contraction and vertical uplift/thickening of the crust have been shown to be the primary method to accommodate deformation between the late Cretaceous and Miocene in the Tibetan Plateau (Chung et al., 1998; Ruddiman, 1998; Royden et al., 2008). Since the middle Miocene, the Tibetan Plateau has exhibited expansion and outward growth (Molnar & Tapponnier, 1975; Royden, 1997, 2008). Contemporary GPS observations identify two significant expansion passages blocked by the Sichuan Basin: 1) the southeastward extrusion around the eastern Himalaya Syntaxis (EHS) despite its dynamic mechanisms and 2) the north-/east-/northeast-ward growth (Zhang et al., 2004; Gan et al., 2007; Wang & Shen, 2020). Unlike the clear extrusion in the southeastern Tibetan Plateau (Bai et al., 2010; Bao et al., 2015; Li et al., 2020; Wang & Shen, 2020), the expansion passage and strain pattern are still under debate within the northeastern Tibetan Plateau.

There are two leading models to explain the expansion and deformation pattern of the northeastern Tibetan Plateau. One model highlights the significance of the eastward extrusion of the crustal materials, which considers the Qinling orogen as the channel for the eastward escape of the plateau materials (Tapponnier, 2001; Ma et al., 2013; Yu & Chen, 2016). The other model suggests bookshelf faulting, governed by the large-scale sinistral Haiyuan and Kunlun faults and the dextral Riyueshan and Elashan faults, in which the deformation induced from the northeast-ward/eastward extrusion of Tibetan Plateau is confined to the plateau and accommodated by complex crustal deformation (i.e., block rotation and tectonic uplift), adjacent to the West Qinling, Qilian, and Liupanshan regions (Cheng et al., 2015; England & Molnar, 1990; Hao et al., 2021; Kirby et al., 2007; Kirby & Harkins, 2013; Li Y. et al., 2018; Zheng et al., 2016; Zuza and Yin, 2016).

Therefore, the West Qinling orogen is pivotal to understand the strain pattern in the northeastern Tibetan Plateau. Previous studies, based on dense horizontal GPS velocities and active tectonics, suggest that the crustal deformation in West Qinling orogen is characterized by crustal contraction, mountain uplift, diffuse deformation, and basin formation (Hao et al., 2021; Kirby et al., 2007; Li Y. et al., 2018; Zheng et al., 2016). However, vertical crustal motions have not been thoroughly investigated, hindering further understanding of the deformation pattern in this region. Hao et al. (2016) proposed a vertical velocity field around the Ordos block, which is inferred from precise leveling observations with a lack of concentration on the contemporary deformation in the West Qinling regions. Additionally, the direct explanation of leveling vertical velocities might be misleading due to the influence of local non-tectonic factors (Hammond et al., 2016; Hao et al., 2016; Hammond et al., 2019).

In this study, a vertical land motion (VLM) model is constructed using a robust imaging method (Hammond et al., 2016; Kreemer et al., 2020) and leveling observations from Hao et al. (2016) with new observations from recent field work. The slip rate and locking coefficients of the West Qinling fault, the longest active fault in West Qinling orogen, are calculated with the GPS velocity field from Hao et al. (2021), and our VLM model. Additionally, the deformation pattern is analyzed based on the 3-D deformation model. This study provides new evidence of strain transformation between horizontal contraction and vertical uplift, which furthers our understanding of the strain pattern in the northeastern Tibetan Plateau.

TECTONIC SETTING

The West Qinling orogen separates the North China block and Lanzhou block from the South China block and Songpan-Ganzi Terrane (**Figures 1A**,**B**; Zheng et al., 2010), and is also recognized as the step-over of the large-scale sinistral Haiyuan and Kunlun faults (**Figure 1**; Yuan et al., 2004), which control the deformation pattern in the northeastern Tibetan Plateau (Kirby et al., 2007; Duvall & Clark, 2010; Yuan et al., 2013; Cheng et al., 2014; Zuza and Yin, 2016). Two small-scale active fault zones, exhibiting low levels of slip, are found along the West Qinling orogen, including the NWW-trending sinistral and NEE-trending dextral fault systems, which signal the diffuse deformation and slip transference along the east end of the Kunlun fault (i.e., Zheng et al., 2016; Zheng et al., 2013).

As the northern boundary of the West Qinling orogen, the nearly W-E striking sinistral West Qinling fault, with a length of ~600 km, separates the Lanzhou (Longxi) block from the West Qinling orogen (**Figure 1B**). The West Qinling fault has experienced a long evolutionary history since the Paleogene. It was initiated as a frontal thrust fault (Clark et al., 2010), and reactivated in the late Quaternary (Li et al., 2007). Field investigations and structural geological data, identify slip rates of ~2.5–2.9 mm/yr (Chen & Lin, 2019), 0.71 ± 0.18 mm/yr (Zheng et al., 2016), and −2.3 ± 0.2 mm/yr (Li et al., 2007) since the Pleistocene. However, contemporary geodetic data indicates slip rates of <1 mm/yr (Hao et al., 2021; Li Y. et al., 2018). Seismic records show that no major earthquakes occurred along the West Qinling fault in the past ~300 years since the 1718 M7.5 Tongwei earthquake.

DATA AND METHODS

GPS horizontal velocities were collected from Hao et al. (2021). The data were obtained from the Crustal Movement Observation Network of China (CMONOC), the National GPS Geodetic Control Network of China (NGGCNC), and the Gansu Bureau of Surveying Mapping and Geoinformation (GBSMG). Parts of the NGGCNC stations were resurveyed by the China Earthquake Administration (CEA) and the Second Monitoring

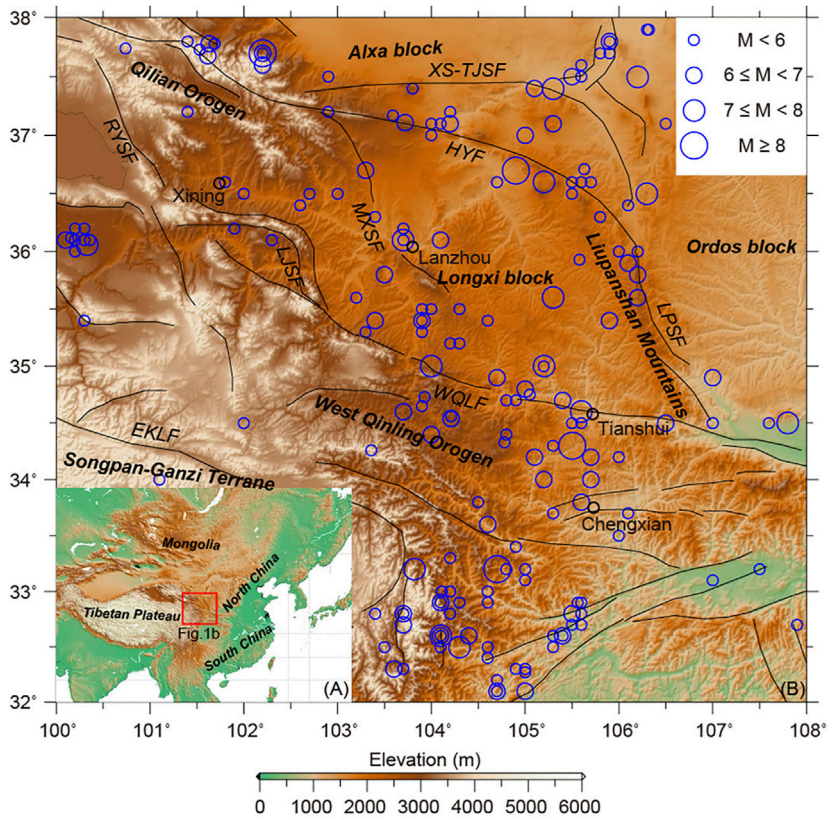

FIGURE 1 | Main tectonic units, active faults, and historic earthquakes with M ≥ 5 since 730 AD from the China Earthquake Datacenter (CEDC) adjacent to the West Qinling Orogen. RYSF: Riyueshan fault; LJSF: Lajishan fault; EKLF: Kunlun fault; MXSF: Maxianshan fault; LPSF: Liupanshan fault; HYF: Haiyuan fault; XS-TJSF: Xiangshan-Tianjingshan fault; WQLF: West Qinling fault.

and Application Center (SMAC). First, the GAMIT package (Herring et al., 2015a) was utilized to process all raw GPS data, containing ~70 International Terrestrial Reference Frame (ITRF) core stations, to obtain loosely daily solutions of satellite orbits, station coordinates, tropospheric zenith delays, and their co-/variances. The geophysical models and parameters used in data processing are shown in Table S1. Second, the GLOBK software (Herring et al., 2015b) was utilized to combine the regional and global daily solutions to estimate station positions and uncertainties, and to convert the loosely daily solutions into the ITRF 2014 (Altamimi et al., 2017). Third, GPS position time series were contaminated by the 2008 *Ms* 8.0 Wenchuan and 2011 *Ms* 9.0 Tohoku-Oki earthquakes (Wang & Shen, 2020). The coseismic displacements from Shen et al. (2009) and Hao and Zhuang, (2020) were therefore interpolated onto GPS sites by utilizing the Kriging method and were used to correct the position time series. Considering the postseismic deformation of the 2008 *Ms* 8.0 Wenchuan earthquake, GPS data measured before 2008 are used for those stations within the postseismic deformation region determined by Wang & Shen (2020). The postseismic deformation of the 2011 Tohoku-Oki earthquake is not significant within our study area, and is thus disregarded. Finally, GPS velocities with respect to ITRF2014 were fitted from the corrected GPS position time series using a linear function (**Equation 1**) and weighted least squares. Here $x(t)$ is the site position time series; x_0 is the initial position at time t_0; v represents station velocity, and D_i is the coseismic (or equipment changes) step at time t_i; $H(t\text{-}t_i)$ is the Heaviside function; n_c is the number of earthquakes and equipment changes. Data are then transformed into a regional reference frame with respect to the stable Ordos block using the rotation pole of (75.083°N ± 0.850°, 139.692°W ± 3.701°, 0.352 ± 0.006°/Ma) (**Figure 2A**) provided by Hao et al. (2021).

$$x(t) = x_0 + v(t - t_0) + \sum D_i \mathrm{H}(t - t_i) \tag{1}$$

Parts of the leveling data in Hao et al. (2016) are included. First-order leveling observations were also collected from the National Administration of Surveying, Mapping and Geoinformation (NASMG) resurveyed in 2013, and 500 km leveling routes in the west of the Ordos block observed in 1985/1986/1994 and resurveyed in 2017 and 2018. Vertical velocities (**Figure 2B**) were calculated following Hao et al. (2016), with 37 stable continuous GPS vertical velocities utilized during leveling adjustment to define the reference frame and to reduce systematic errors accumulated during leveling routes (see Hao et al. (2016) for more details). Since the leveling data are sensitive to local environmental effects, such

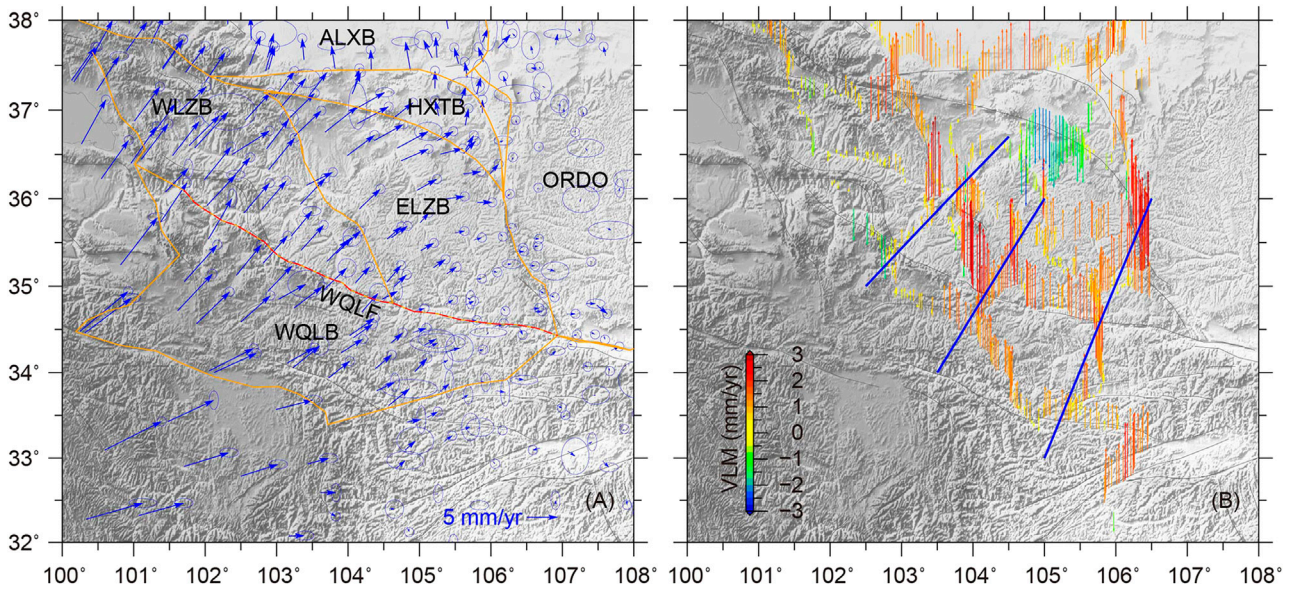

FIGURE 2 | (A) GPS velocity field, relative to the Ordos block, and block models used in this study's inversion. Orange lines indicate block boundaries and the red dashed line denotes the west Qinling active fault. **(B)** Vertical velocities derived from leveling observations. Three blue lines correspond to the profiles presented in **Figure 5**. WLZB: the west Lanzhou (Longxi) block, ELZB: the east Lanzhou (Longxi) block; ORDO: the Ordos block; WQLB: the west Qinling block; ALXB: the Alxa block; HXTB: the block between the Haiyuan and Xiangshan-Tianjingshan faults; WQLF: the west Qinling fault.

as groundwater changes and human activities (Hammond et al., 2016; Hao et al., 2016), we therefore despeckle the velocities with GPS-Imaging, which is robust against outliers, to construct a spatially smoothed VLM model (Hammond et al., 2016; Kreemer et al., 2020; **Figures 3B**, **Supplementary Figure S1**).

RESULTS

Horizontal Deformation From GPS Observations

The GPS horizontal velocity field, with respect to the Ordos block, identifies NNE-directed crustal movement, with significant velocity gradients adjacent to the sinistral Haiyuan and Kunlun faults but not along the West Qinling fault (**Figure 2A**), which suggests large horizontal differential motions along the former faults. Moreover, the velocity vectors decrease significantly to the east of 105°–106°E. To investigate these large velocity gradient belts, the strain rate field is calculated utilizing the Median Estimation of Local Deformation (MELD) algorithm, which is robust against outliers and provides realistic uncertainties (Kreemer et al., 2018, 2020). MELD requires two parameters to calculate the strain rates at grid points from the multivariate median of a set of strain rates from a number of station-based local triangles. The first parameter is the minimum number of the triangles (N_{min}), which we set here to be N_{min} = 56, meaning as few as 6 stations can be used to calculate strain rates. The second parameter is the maximum allowed value of σ_{max}, which is based on the theoretical standard deviation in the strain rate for a triangle of stations, based on the triangle's geometry and size. This parameter is used to exclude triangles that are too small and skinny and would be detrimental to the results (Kreemer et al., 2018, 2020). We use $\sigma_{max} = 15 \times 10^{-9}$/yr, which is chosen to calculate the strain rates with a minimum theoretical spatial resolution of ~40 km (**Figure 3D**).

The maximum shear strain rates are 0–30 × 10^{-9}/yr with the largest value existing along the Haiyuan and Kunlun faults (background in **Figure 3A**). These results are consistent with those of Hao and Zhuang, (2020) and Wang & Shen (2020). The dilatation strain rates are −15–15 × 10^{-9}/yr and are dominantly characterized by contraction, with the peak values appearing along the West Qinling and the Qilian orogens (**Figure 3B**). The principal strain rates are oriented with E-/NE-directed contraction and N-/NW-directed extension (**Figure 3A**). In addition, strain rates significantly decrease to the east of 105°–106°E (similar with the GPS velocity field, background in **Figures 3A**,**B**), which may identify the significant deformation regions accommodating the outward expansion of the northeastern Tibetan Plateau (at least in the upper crust) resulting from India-Eurasia convergence being blocked by the rigid Ordos block. The rotation rates in **Figure 3C** (background color) show the clockwise rotation of the West Qinling orogen and the Lanzhou (Longxi) sub-blocks and the anticlockwise rotation of the sub-blocks adjacent to the Haiyuan and Kunlun faults, which are required by the book-shelf kinematic model (i.e., Zuza and Yin, 2016; Cheng et al., 2021).

Vertical Land Motion

The proposed VLM model in **Figure 3B**, **Supplementary Figure S1** shows that the northeastern Tibetan Plateau uplifts at a rate of 0–3 mm/yr, except for the northeastern portion of the east

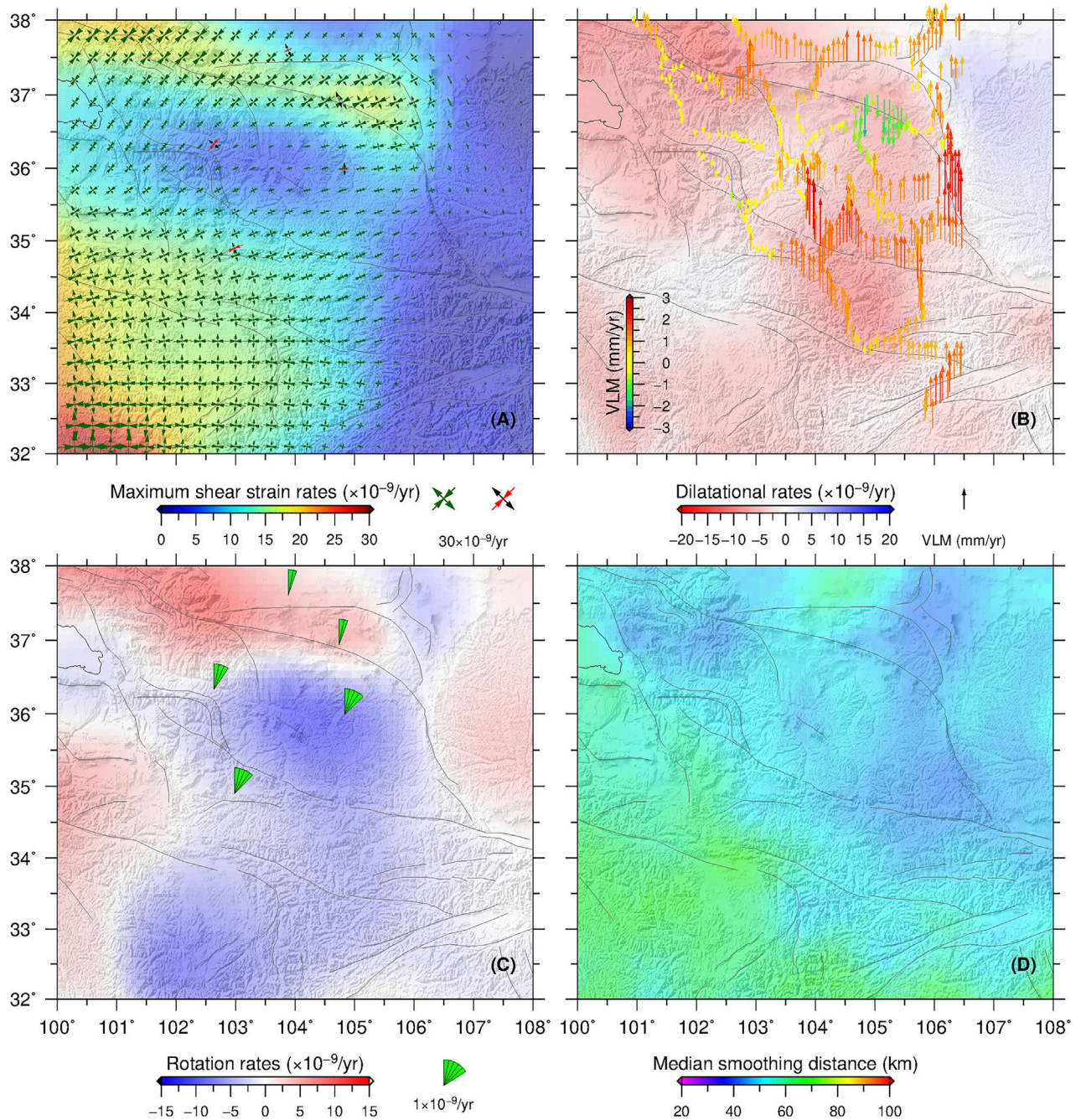

FIGURE 3 | (A) Principal strain rates (darkgreen arrows) and the maximum shear strain rates (background color). Black and red arrows correspond to the block internal principal strain rates determined from TDEFNODE. **(B)** Dilatational strain rates (background color, with the warm color indicating contraction and the cold color denoting dilatation) and vertical land motion model (arrows). **(C)** Rotation rates. Red denotes an anticlockwise rotation, and blue indicates a clockwise rotation. The green fan denotes the rotation rate determined from block models. **(D)** Median smoothing distance.

Lanzhou sub-block (ELZB), where a series of Cenozoic pull-apart basins are present (e.g., the Tianzhu and Ganyanchi basins) due to the sinistral strike-slip of the Haiyuan fault (Tian et al., 2002). The largest uplift rates appear along the Liupanshan fault, which is regarded as the northeastern margin of the outward expansion of the Tibetan Plateau (Li et al., 2017; Du et al., 2018), and the transpressional structure of the Haiyuan active fault to accommodate its sinistral motions (Zheng et al., 2013). Meanwhile, substantial uplift is observed between the central and eastern segments of the West Qinling orogen and the ELZB block, accompanied by large horizontal compression (**Figure 3B**). In the western Lanzhou block (WLZB), the uplift rate is much

smaller than that in the ELZB block, which indicates that the strong contraction along the Lajishan fault (LJSF) is transmitted to the Maxianshan fault (MXSF) and/or even further east. The uplift rates along the northern side of the Haiyuan fault are 1–2 mm/yr.

Rigid Block Rotation, Fault Coupling, and Block Internal Deformation

We simultaneously estimate the angular velocities and permanent strain rates within the (sub-) blocks and fault locking parameters of the West Qinling fault using the TDEFNODE program (McCaffrey et al. (2007)). To accomplish this, the study area is divided into seven small (sub-) blocks according to the distribution of active faults and seismicity (**Figures 1**, **2A**): 1) the Ordos block (ORDB, regarded as the reference frame in our inversion), 2) the WLZB, 3) the ELZB, 4) the Alxa block (ALXB), 5) the West Qinling block (WQLB), and 6) the smallest block between the Haiyuan and Xiangshan-Tianjingshan faults (HXTB). Slip vectors (***V***) of the active fault can be calculated from the angular velocities of adjacent blocks.

In TDENODE, the interseismic elastic deformation adjacent to the fault is denoted by φ (the locking coefficient), which is a purely kinematic, unitless quantity, that represents the instantaneous, spatially averaged creep fraction. $\varphi = 0$ signifies a fully creeping fault, while $\varphi = 1$ indicates a completely locked fault. A φ value between 0 and 1 suggests that the fault is partially locked. Faults are represented in 3-D by nodes distributed on the surface, which is parameterized by longitude, latitude, and depth. The values of φ and slip deficit, defined as $\varphi \boldsymbol{V}$, are calculated at each node.

Block angular velocities, average strain rates, and fault coupling coefficients (φ) are determined using the non-linear simulated annealing and grid search approaches constrained with geodetic observations (McCaffrey et al., 2007). The goodness of fit of a particular set of parameters is based on the reduced χ^2 statistics (**Eq. 2**):

$$\chi_n^2 = (N - P)^{-1} \sum_{1}^{N} p_i, \tag{2}$$

where N is the number of observations, P is the number of free parameters, and p_i is the misfit penalty function defined by the ratio between the data fitting residuals and data uncertainties. In the inversion, 279 horizontal GPS vectors and 514 vertical rates, derived from leveling observations, are used.

The χ^2 values are 1.03 and 2.1 for the horizontal GPS and vertical velocities respectively, with residuals of horizontal GPS and vertical leveling velocities smaller than 2 mm/yr (**Supplementary Figure S2**). These values are similar to the observed data standard deviations and suggest reliable inversion results. TDEFNODE can only remove an average regional uplift and model uplift due to the locking on the faults (McCaffrey, 2005), resulting in a poor fit to the vertical velocities. **Figures 3A,C** present the rotation rates and internal deformation of the (sub-) blocks. The internal permanent strain rates of each (sub-) block (red arrows in **Figure 3A**) are pretty

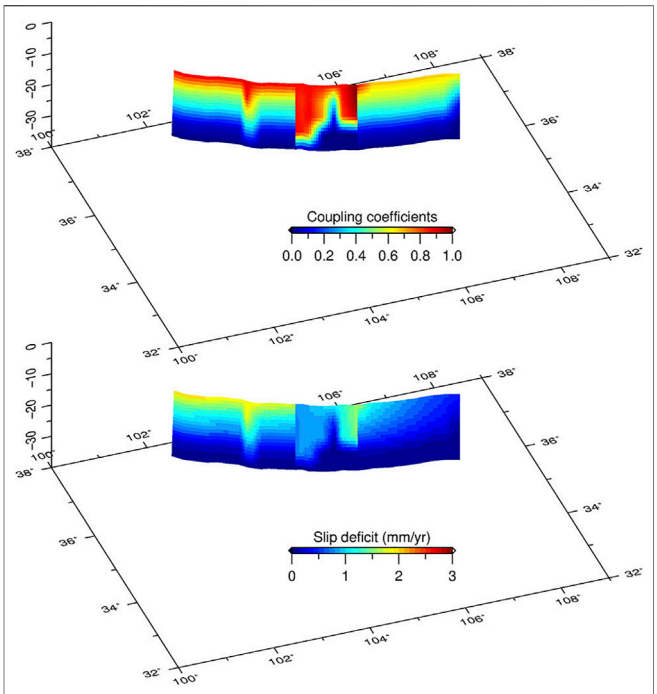

FIGURE 4 | (A) Locking coefficients and **(B)** slip deficit of the WQLF (west Qinling fault) calculated from TDEFNODE and constrained with GPS and VLM observations.

similar to the strain rates calculated from MELD (dark green arrows in **Figure 3A**). Our results identify clockwise rotations of the ELZB, WLZB, and WQLB relative to the ORDO block with rotation rates of −0.028°/Myr, −0.063°/Myr, −0.040°/Myr (green fans in **Figure 3C**, with negative value indicating clockwise rotation), with the exception of the ALXA block. **Figures 4A,B** show the locking coefficients and slip deficit of the West Qinling fault. Average locking depths of the West Qinling fault are 6.6, 6.8, and 6.1 km from west to east with slip deficits of 1.2 mm/yr, 1.1 mm/yr, and 1.1 mm/yr respectively. In **Figures 4**, the regions of strongest coupling are located within the central and the western segments of the West Qinling fault, suggesting high seismic risks (Ma et al., 2017).

DISCUSSION

Slip Rates and Seismicity of the West Qinling Fault

Slip rates of 1.5 ± 0.4 mm/yr to 1.7 ± 0.3 mm/yr are identified for the West Qinling fault, which are larger than previous geodetic and geologic evidence-based estimates of 0.4 ± 0.3 mm/yr (Hao and Zhuang, 2020), 0.71 ± 0.18 mm/yr (Zheng et al., 2016), and 0.8 mm/yr (Li Y. et al., 2018). However, these values are smaller than the geologically derived slip rates of 2–3 mm/yr (Li et al., 2007; Chen & Lin, 2019). Slip rates of the West Qinling fault are far smaller than other NWW-directed sinistral active faults within the region, such as the Kunlun fault, which exhibits slip of 2.0 ± 0.4 mm/yr along its eastern segment to

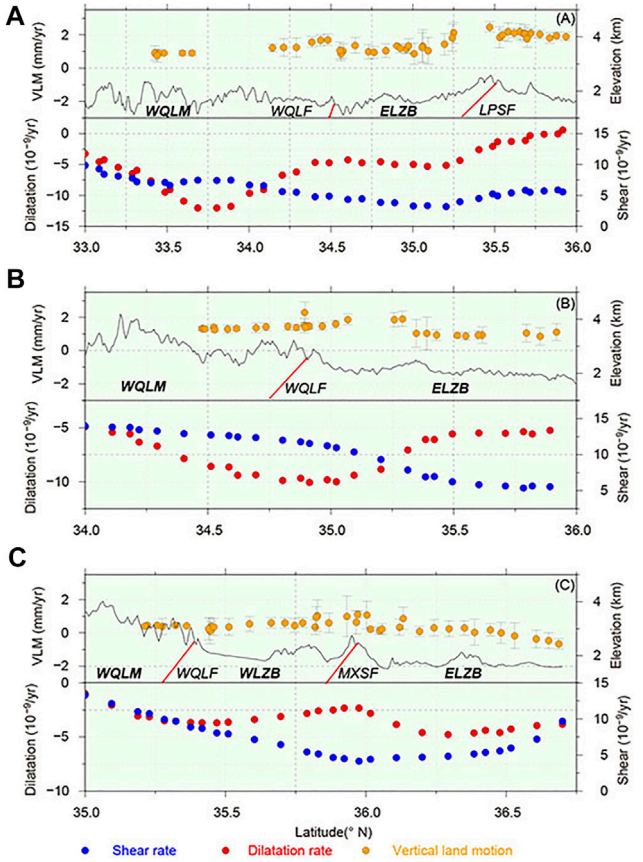

FIGURE 5 | Strain rate (dilatation and shear) and VLM (Vertical Land Motion) profiles perpendicular to the west Qinling fault. **(A,B,C)** represent the east, central, and west profiles in **Figure 2B**, respectively. Blue, red, and orange dots denote the shear strain rate, dilatation strain rate, and uplift rates. The red bold lines represent the active faults. The gray bold line denotes the topography. WQLM: west Qinling Mountains, WQLF: the west Qinling fault; ELZB: the east Lanzhou block; LPSF: the Liupanshan fault; WLZB: the west Lanzhou fault; MXSF: the Maxianshan fault.

~16 mm/yr along its western segment (Kirby et al., 2007; Harkins & Kirby, 2008; Harkins et al., 2010; Loveless & Meade, 2011), and the Haiyuan fault with 1–3 mm/yr along the western segment to 8–10 mm/yr along the eastern segment (Hao and Zhuang, 2020; Li Y. et al., 2018; Loveless & Meade, 2011; Yao et al., 2019; Yuan et al., 2013). The slow slip of the West Qinling fault can be related to limited convergence transfer and that a majority of the strain has likely been absorbed and partitioned by crustal shortening, block rotation, and east-west stretching along the West Qinling orogen (Chen & Lin, 2019; Cheng et al., 2021; Zheng et al., 2016).

Due to the lack of major earthquakes in the last 300 years, the seismic risk of the West Qinling fault has drawn much attention in recent decades. Wang et al. (2011) suggested that there is an *Mw*7.7 moment magnitude deficit in the last 400 years. However, this study might overestimate the slip rate of the West Qinling fault with a value of 2–3 mm/yr, which is 3.7 ± 1.8 mm/yr, compared to results in these few years based on modern dense GPS observations (i.e., Hao and Zhuang, 2020; Li Y. et al., 2018).

In this study, the moment deficit of the West Qinling fault is recalculated according to the equation, $M_0 = \mu DA$, based on the determined average locking depth and slip deficit (**Figure 4**), where the shear modulus is assumed to be 30 GPa. This yields an accumulated seismic moment of 1.8×10^{20} N·m (or 1.35×10^{20} N·m) for the past 400 (or 300) years, corresponding to an earthquake with a moment magnitude of *Mw*7.4 (or *Mw*7.35), which is smaller than estimated by Wang et al. (2011).

Strain Transformation and Tectonic Uplift Adjacent to the West Qinling Orogen

Three coexisting end-member models exist to explain the uplift mechanism of the northeastern Tibetan Plateau, where the West Qinling orogen and Liupanshan Mountains are included: 1) strain transformation from horizontal contraction to vertical uplift induced from India-Eurasia oblique convergence (e.g., Tapponnier, 2001; Allen et al., 2017), 2) eastward flow of middle-to-lower crustal materials (Royden, 1997; Royden et al., 2008; Wang et al., 2018), and 3) changes in the balance between stress gradients and body forces, resulting from the removal of lithospheric materials due to asthenospheric flow, and have produced significant topographic relief (England & Houseman, 1989; Molnar et al., 1993; Ye et al., 2017). The latest, dense 3-D geodetic observations provide a new opportunity to reanalyze these models. To identify contemporary crustal deformation features in this region, three vertical velocity and horizontal strain rate profiles are produced, together with the topography along the West Qinling Mountains normal to the West Qinling fault (**Figures 2B**, **5**).

The profiles identify contraction strain rates (red dots in **Figure 5**) ranging between 0 and -12.5×10^{-9}/yr combined with 1–2 mm/yr of uplift (orange dots with gray bars in **Figure 5**), suggesting transformation of strain from crustal contraction to vertical uplift. Assuming that the volume is conserved, the sum of the three principal strain rates should be zero, and contraction should be equal to, or at least proportional to, uplift (Lease et al., 2012; Ge et al., 2015). Considering a crustal thickness of ~50 km in the northeastern Tibetan Plateau (Guo & Chen, 2017; Ye et al., 2017), the observed contraction can produce maximum uplift of 0.625 mm/yr, consistent with the <1 mm/yr from continuous GPS observations (Su et al., 2018), but smaller than 1–2 mm/yr from our VLM model.

Volumetric conservation requires consistency between the crustal contraction and uplift, however, the opposite relationship is observed in **Figure 5**, where the largest contraction occurs along with the smallest uplift (at the lowest elevations) and vice versa, especially adjacent to the West Qinling and Liupanshan Mountains, which are also presented in GPS vertical velocities (Su et al., 2018). A possible explanation may come from the different origins of vertical lithospheric stress. To analyze the lithospheric flexure mechanism in the northeastern Tibetan Plateau, Wang et al. (2018) and She et al. (2016) estimated the effective elastic thickness (Te) and loading ratios based on Gravity and GPS hybrid measurements. Their results show that loading ratios of the West Qinling orogen (F1 = 0.19, F2 = 0.42 and F3 = 0.39), with F1, F2 and F3 implying initial

loading resulting from the Earth's surface, the interface between the upper and lower crust, and the Moho, suggesting that the initial loading is primarily attributed to the lower crust (i.e., lower crustal materials flow); however, loading ratio of the Liupanshan Mountains (F1 = 0.95; F2 = 0.05; F3 = 0) indicates that initial loading is primarily attributed to the surface (i.e., strain transformation from crustal contraction to uplift/thickening). Although the existence of middle-to-lower crustal material flow and its contributions to tectonic uplift remain contested (e.g., Lease et al., 2012), seismic tomography identifies complex deep structures beneath the West Qinling orogen and Liupanshan Mountains, i.e., low S-wave velocity underneath the West Qinling orogen at depths of 15–30 km (Yang et al., 2012), low shear-wave velocity in the middle-lower crust but high seismic velocity in the upper crust beneath the West Qinling orogen (Bao et al., 2013), a broad low-velocity zone in the middle-to-lower crust beneath the northeastern Tibetan Plateau (Guo & Chen, 2017; Li S. et al., 2018; Ye et al., 2017), and a complex double Moho structure exists induced from the superposition of the rigid Ordos and the relatively soft northeastern Tibet crust (Li et al., 2017). Therefore, despite quantifying relative contributions from different mechanisms of lithospheric flexure, which still require further investigation (i.e., She et al., 2017; Wang et al., 2018), this study suggests that the strain transformation in the upper crust and complex middle-to-lower crustal structures underneath, control the complex tectonic uplift and geomorphologic/topographic features adjacent to the West Qinling Orogen; i.e., generation of two sets of small-scale active faults, development of several Cenozoic basins (e.g., the Guide, Tongren, Wushan basins; Zheng et al., 2016), and the uplift of the West Qinling Mountains.

Implications for the Outward Growth of the Northeastern Tibetan Plateau

The expansion direction and passage of the northeastern Tibetan Plateau have been contested for decades. In one aspect, some studies suggest that the crustal materials in the northeastern Tibetan Plateau are escaping eastward along the Qinling Mountains and/or beneath the Ordos block (Li S. et al., 2018; Royden et al., 2008; Royden, 1997; Yu & Chen, 2016). Meanwhile, others highlight that the deformation is mainly limited within the plateau and is accommodated by crustal shortening, block rotation, fault movements, and mountain building (Cheng et al., 2015, 2021; Hao et al., 2021; Kirby et al., 2007; Li Y. et al., 2018; Zheng et al., 2016; Zuza and Yin, 2016).

The 3-D crustal deformation model presented in this study indicates that crustal deformation in the northeastern Tibetan plateau is primarily characterized by horizontal contraction, as large as 15×10^{-9}/yr, as well as vertical uplift/thickening, with the magnitude of 0–3 mm/yr. GPS velocities, with respect to the Ordos block, show significant NNE-ward crustal movement instead of eastward materials escape. These observations support the latter and highlight the importance of strain transformation between horizontal crustal shortening and vertical uplift to accommodate crustal deformation induced from outward growth of the northeastern Tibetan Plateau. Additionally, middle-to-lower crustal material expansion (e.g., middle-to-lower crustal flow) may also have some contributions, especially underneath the West Qinling orogen, which requires further investigations to confirm. Both strain rates and GPS velocities identify a deformation gradient belt at longitudes 105°–106°E, which distinguish significant deformation regions accommodating outward expansion of the northeastern Tibetan Plateau. While we are unable to exclude potential contributions of eastward materials escape, it appears to be inconsequential to our 3-D crustal deformation model (**Figures 2A**, **3A**,**B**).

CONCLUSION

This study constructed a VLM model based on leveling observations adjacent to the West Qinling orogen, identifying uplift rates of 0–3 mm/yr within this region. Combined with the horizontal strain rate field, this study suggests that strain transformation has played an important role in controlling the tectonic uplift of the West Qinling orogen. Moreover, slip rate and locking coefficients were inverted and the moment deficit of the West Qinling fault was calculated. The West Qinling fault slips slowly at a rate of 1–2 mm/yr and is strongly locked with average locking depths of 6.6, 6.8, and 6.1 km in its western, central, and eastern segments. This equates to a moment magnitude deficit of *Mw*7.4. Additionally, results identify a significant deformation transition belt at the longitude of 105°–106°E, which indicates that the deformation of the northeastern Tibetan Plateau is primarily limited to within the plateau, rather than being accommodated by crustal materials that are escaping eastward along the Qinling orogen.

DATA AVAILABILITY STATEMENT

The raw data supporting the conclusions of this article will be made available by the authors, without undue reservation.

AUTHOR CONTRIBUTIONS

ZL designed the study and did all the calculations in the paper. ZL wrote the paper, with contributions of FC and ZY. MH and WZ processed the GPS data. SS and FY processed the leveling data.

FUNDING

This work got funded by the National Key Research and Development Program of China (2017YFC1500102) and National Natural Science Foundation of China (42002234, 41874017, 41474090, and 41874024).

ACKNOWLEDGMENTS

We sincerely thank Associate Editor David K. Wright and two reviewers for their help improving the manuscript. We

thank all the staff of Crustal Movement Observation Network of China (CMONOC), the National GPS Geodetic Control Network of China (NGGCNC), the Gansu Bureau of Surveying Mapping and Geoinformation (GBSMG), and the National Administration of Surveying, Mapping and Geoinformation (NASMG) for their hardworking to get the data. All figures were created using Generic Mapping Tools (Wessel and Smith, 1998). The Earthquake catalogs are from China Earthquake Datacenter (http://data.earthquake.cn/) and GCMT (https://www.globalcmt.org/).

SUPPLEMENTARY MATERIAL

The Supplementary Material for this article can be found online at: https://www.frontiersin.org/articles/10.3389/feart.2021.689087/full#supplementary-material

REFERENCES

Allen, M. B., Walters, R. J., Song, S., Saville, C., De Paola, N., Ford, J., et al. (2017). Partitioning of Oblique Convergence Coupled to the Fault Locking Behavior of Fold-And-Thrust Belts: Evidence from the Qilian Shan, Northeastern Tibetan Plateau. *Tectonics* 36 (9), 1679–1698. doi:10.1002/2017TC004476

Altamimi, Z., Métivier, L., Rebischung, P., Rouby, H., and Collilieux, X. (2017). ITRF2014 Plate Motion Model. *Geophys. J. Int.* 209, 1906–1912. doi:10.1093/gji/ggx136

Bai, D., Unsworth, M. J., Meju, M. A., Ma, X., Teng, J., Kong, X., et al. (2010). Crustal Deformation of the Eastern Tibetan Plateau Revealed by Magnetotelluric Imaging. *Nat. Geosci.* 3 (5), 358–362. doi:10.1038/ngeo830

Bao, X., Song, X., Xu, M., Wang, L., Sun, X., Mi, N., et al. (2013). Crust and Upper Mantle Structure of the North China Craton and the NE Tibetan Plateau and its Tectonic Implications. *Earth Planet. Sci. Lett.* 369-370, 129–137. doi:10.1016/j.epsl.2013.03.015

Bao, X., Sun, X., Xu, M., Eaton, D. W., Song, X., Wang, L., et al. (2015). Two Crustal Low-Velocity Channels beneath SE Tibet Revealed by Joint Inversion of Rayleigh Wave Dispersion and Receiver Functions. *Earth Planet. Sci. Lett.* 415, 16–24. doi:10.1016/j.epsl.2015.01.020

Chen, P., and Lin, A. (2019). Tectonic Topography and Late Pleistocene Activity of the West Qinling Fault, Northeastern Tibetan Plateau. *J. Asian Earth Sci.* 176, 68–78. doi:10.1016/j.jseaes.2019.02.007

Cheng, F., Jolivet, M., Dupont-Nivet, G., Wang, L., Yu, X., and Guo, Z. (2015). Lateral Extrusion along the Altyn Tagh Fault, Qilian Shan (NE Tibet): Insight from a 3D Crustal Budget. *Terra Nova* 27 (6), 416–425. doi:10.1111/ter.12173

Cheng, F., Jolivet, M., Fu, S., Zhang, Q., Guan, S., Yu, X., et al. (2014). Northward Growth of the Qimen Tagh Range: A New Model Accounting for the Late Neogene Strike-Slip Deformation of the SW Qaidam Basin. *Tectonophysics* 632, 32–47. doi:10.1016/j.tecto.2014.05.034

Cheng, F., Zuza, A. V., Haproff, P. J., Wu, C., Neudorf, C., Chang, H., et al. (2021). Accommodation of India-Asia Convergence via Strike-Slip Faulting and Block Rotation in the Qilian Shan Fold-Thrust belt, Northern Margin of the Tibetan Plateau. *J. Geol. Soc.* 178, jgs2020–207. doi:10.1144/jgs2020-207

Chung, S.-L., Lo, C.-H., Lee, T.-Y., Zhang, Y., Xie, Y., Li, X., et al. (1998). Diachronous Uplift of the Tibetan Plateau Starting 40?Myr Ago. *Nature* 394 (6695), 769–773. doi:10.1038/29511

Clark, M. K., Farley, K. A., Zheng, D., Wang, Z., and Duvall, A. R. (2010). Early Cenozoic Faulting of the Northern Tibetan Plateau Margin from Apatite (U-Th)/He Ages. *Earth Planet. Sci. Lett.* 296 (1), 78–88. doi:10.1016/j.epsl.2010.04.051

Du, F., Wen, X., Feng, J., Liang, M., Long, F., and Wu, J. (2018). Seismo-tectonics and Seismic Potential of the Liupanshan Fault Zone (LPSFZ), China. *Chin. J. Geophys.* 61 (2), 545–559. (in Chinese with English abstract). doi:10.6038/cjg2018L0181

Duvall, A. R., and Clark, M. K. (2010). Dissipation of Fast Strike-Slip Faulting within and beyond Northeastern Tibet. *Geology* 38 (3), 223–226. doi:10.1130/G30711.1

England, P., and Houseman, G. (1989). Extension during continental Convergence, with Application to the Tibetan Plateau. *J. Geophys. Res.* 94 (B12), 17561. doi:10.1029/JB094iB12p17561

England, P., Houseman, G., and Sonder, L. (1985). Length Scales for continental Deformation in Convergent, Divergent, and Strike-Slip Environments: Analytical and Approximate Solutions for a Thin Viscous Sheet Model. *J. Geophys. Res.* 90 (B5), 3551. doi:10.1029/JB090iB05p03551

England, P., and Molnar, P. (1990). Right-lateral Shear and Rotation as the Explanation for Strike-Slip Faulting in Eastern Tibet. *Nature* 344 (6262), 140–142. doi:10.1038/344140a0

Gan, W., Zhang, P., Shen, Z.-K., Niu, Z., Wang, M., Wan, Y., et al. (2007). Present-day Crustal Motion within the Tibetan Plateau Inferred from GPS Measurements. *J. Geophys. Res.* 112 (B8), B08416. doi:10.1029/2005JB004120

Ge, W.-P., Molnar, P., Shen, Z.-K., and Li, Q. (2015). Present-day Crustal Thinning in the Southern and Northern Tibetan Plateau Revealed by GPS Measurements. *Geophys. Res. Lett.* 42 (13), 5227–5235. doi:10.1002/2015GL064347

Guo, Z., and Chen, Y. J. (2017). Mountain Building at Northeastern Boundary of Tibetan Plateau and Craton Reworking at Ordos Block from Joint Inversion of Ambient Noise Tomography and Receiver Functions. *Earth Planet. Sci. Lett.* 463, 232–242. doi:10.1016/j.epsl.2017.01.026

Hammond, W. C., Blewitt, G., and Kreemer, C. (2016). GPS Imaging of Vertical Land Motion in California and Nevada: Implications for Sierra Nevada Uplift. *J. Geophys. Res. Solid Earth* 121 (10), 7681–7703. doi:10.1002/2016JB013458

Hammond, W. C., Kreemer, C., Zaliapin, I., and Blewitt, G. (2019). Drought-Triggered Magmatic Inflation, Crustal Strain, and Seismicity Near the Long Valley Caldera, Central Walker Lane. *J. Geophys. Res. Solid Earth* 124 (6), 6072–6091. doi:10.1029/2019JB017354

Hao, M., Li, Y., Wang, Q., Zhuang, W., and Qu, W. (2021). Present-Day Crustal Deformation within the Western Qinling Mountains and its Kinematic Implications. *Surv. Geophys.* 42 (1), 1–19. doi:10.1007/s10712-020-09621-5

Hao, M., Wang, Q., Cui, D., Liu, L., and Zhou, L. (2016). Present-Day Crustal Vertical Motion Around the Ordos Block Constrained by Precise Leveling and GPS Data. *Surv. Geophys.* 37 (5), 923–936. doi:10.1007/s10712-016-9375-1

Hao, M., and Zhuang, W. Q. (2020). The Impact of the Great 2011 Tohoku-Oki Earthquake on Crustal Deformation in Eastern China. *Geodesy and Geodynamics* 40 (6), 138–142. (in Chinese with English Abstract). doi:10.14075/j.jgg.2020.06.002

Harkins, N., and Kirby, E. (2008). Fluvial Terrace Riser Degradation and Determination of Slip Rates on Strike-Slip Faults: An Example from the Kunlun Fault, China. *Geophys. Res. Lett.* 35 (5), L05406. doi:10.1029/2007GL033073

Harkins, N., Kirby, E., Shi, X., Wang, E., Burbank, D., and Chun, F. (2010). Millennial Slip Rates along the Eastern Kunlun Fault: Implications for the Dynamics of Intracontinental Deformation in Asia. *Lithosphere* 2 (4), 247–266. doi:10.1130/L85.1

Herring, T. A., King, R. W., and McClusky, S. C. (2015b). *GAMIT Reference Manual, Global Kalman Filter VLBI and GPS Analysis Program*. Cambridge: Massachusetts Institute of Technology. Release 10.6.

Herring, T. A., King, R. W., and McClusky, S. C. (2015a). *GAMIT Reference Manual, GPS Analysis at MIT*. Cambridge: Massachusetts Institute of Technology. Release10.6.

Kirby, E., and Harkins, N. (2013). Distributed Deformation Around the Eastern Tip of the Kunlun Fault. *Int. J. Earth Sci.* 102, 1759–1772. doi:10.1007/s00531-013-0872-x

Kirby, E., Harkins, N., Wang, E., Shi, X., Fan, C., and Burbank, D. (2007). Slip Rate Gradients along the Eastern Kunlun Fault: KUNLUN FAULT, SLIP RATE, TIBET. *Tectonics* 26 (2), na. doi:10.1029/2006TC002033

Kreemer, C., Blewitt, G., and Davis, P. M. (2020). Geodetic Evidence for a Buoyant Mantle Plume beneath the Eifel Volcanic Area, NW Europe. *Geophys. J. Int.* 222 (2), 1316–1332. doi:10.1093/gji/ggaa227

Kreemer, C., Hammond, W. C., and Blewitt, G. (2018). A Robust Estimation of the 3-D Intraplate Deformation of the North American Plate from GPS. *J. Geophys. Res. Solid Earth* 123 (5), 4388–4412. doi:10.1029/2017JB015257

Lease, R. O., Burbank, D. W., Zhang, H., Liu, J., and Yuan, D. (2012). Cenozoic Shortening Budget for the Northeastern Edge of the Tibetan Plateau: Is Lower

Crustal Flow Necessary?: NE Tibetan PLATEAU CRUSTAL SHORTENING. *Tectonics* 31 (3), na. doi:10.1029/2011TC003066

Li, C. Y., Zhang, P. Z., Zhang, J. X., Yuan, D. Y., and Wang, Z. C. (2007). Late-Quaternary Activity and Slip Rate of the Western Qinling Fault Zone at Huangxianggou Segment. *Qua. Sci.* 27, 54–63. (in Chinese with English abstract). doi:10.1016/S1872-5791(07)60044-X

Li, S., Guo, Z., Chen, Y. J., Yang, Y., and Huang, Q. (2018a). Lithospheric Structure of the Northern Ordos from Ambient Noise and Teleseismic Surface Wave Tomography. *J. Geophys. Res. Solid Earth* 123, 6940–6957. doi:10.1029/2017JB015256

Li, W., Gao, R., Wang, H., Li, Y., Li, H., Hou, H., et al. (2017). Crustal Structure beneath the Liupanshan Fault Zone and Adjacent Regions. *Chin. J. Geophys.* 60 (6), 2265–2278. (in Chinese with English abstract). doi:10.6038/cjg20170619

Li, Y., Liu, M., Wang, Q., and Cui, D. (2018b). Present-day Crustal Deformation and Strain Transfer in Northeastern Tibetan Plateau. *Earth Planet. Sci. Lett.* 487, 179–189. doi:10.1016/j.epsl.2018.01.024

Li, Z., Wang, Y., Gan, W., Fang, L., Zhou, R., Seagren, E. G., et al. (2020). Diffuse Deformation in the SE Tibetan Plateau: New Insights from Geodetic Observations. *J. Geophys. Res. Solid Earth* 125 (10). doi:10.1029/2020JB019383

Loveless, J. P., and Meade, B. J. (2011). Partitioning of Localized and Diffuse Deformation in the Tibetan Plateau from Joint Inversions of Geologic and Geodetic Observations. *Earth Planet. Sci. Lett.* 303 (1–2), 11–24. doi:10.1016/j.epsl.2010.12.014

Ma, H., Wu, Y., Feng, J. G., Xu, R., Wu, S., and Wang, Q. (2017). Research on Recent GPS Crustal Deformation Characteristics in the Northeastern Edge of Qinghai-Tibet Plateau. *J. Phys. Conf. Ser.* 910, 012028. doi:10.1088/1742-6596/910/1/012028

Ma, S. X., Zhang, Y. Q., Li, H. L., and Li, J. H. (2013). The Tectonic Extrusion of NE Tibet in Late Neogene Time: Evidence from Anhua-Chengxian basin in West Qinling. *Earth Sci. Front.* 20 (4), 58–74. (in Chinese with English abstract).

McCaffrey, R. (2005). Block Kinematics of the Pacific-North America Plate Boundary in the Southwestern United States from Inversion of GPS, Seismological, and Geologic Data. *J. Geophys. Res.* 110 (B7), B07401. doi:10.1029/2004JB003307

McCaffrey, R., Qamar, A. I., King, R. W., Wells, R., Khazaradze, G., Williams, C. A., et al. (2007). Fault Locking, Block Rotation and Crustal Deformation in the Pacific Northwest. *Geophys. J. Int.* 169 (3), 1315–1340. doi:10.1111/j.1365-246X.2007.03371.x

Molnar, P., England, P., and Martinod, J. (1993). Mantle Dynamics, Uplift of the Tibetan Plateau, and the Indian Monsoon. *Rev. Geophys.* 31 (4), 357. doi:10.1029/93RG02030

Molnar, P., and Tapponnier, P. (1975). Cenozoic Tectonics of Asia: Effects of a Continental Collision: Features of Recent continental Tectonics in Asia Can Be Interpreted as Results of the India-Eurasia Collision. *Science* 189 (4201), 419–426. doi:10.1126/science.189.4201.419

Reilinger, R., McClusky, S., Vernant, P., Lawrence, S., Ergintav, S., Cakmak, R., et al. (2006). GPS Constraints on continental Deformation in the Africa-Arabia-Eurasia continental Collision Zone and Implications for the Dynamics of Plate Interactions: EASTERN MEDITERRANEAN ACTIVE TECTONICS. *J. Geophys. Res. Solid Earth* 111 (B5), na. doi:10.1029/2005JB004051

Royden, L. H., Burchfiel, B. C., King, R. W., Wang, E., Chen, Z., Shen, F., et al. (1997). Surface Deformation and Lower Crustal Flow in Eastern Tibet. *Science* 276 (5313), 788–790. doi:10.1126/science.276.5313.788

Royden, L. H., Burchfiel, B. C., and van der Hilst, R. D. (2008). The Geological Evolution of the Tibetan Plateau. *Science* 321 (5892), 1054–1058. doi:10.1126/science.1155371

Ruddiman, W. (1998). Early Uplift in Tibet?. *Nature* 394, 723–725. doi:10.1038/29401

She, Y., Fu, G., Su, X., Meng, G., Zhu, Y., Guo, S., et al. (2016). Crustal Isostasy and Uplifting Mechanism of the Liupanshan Area. *Prog. Geophys.* 31 (4), 1464–1472. (in Chinese with English abstract). doi:10.6038/pg20160408

Shen, Z.-K., Sun, J., Zhang, P., Wan, Y., Wang, M., Bürgmann, R., et al. (2009). Slip Maxima at Fault Junctions and Rupturing of Barriers during the 2008 Wenchuan Earthquake. *Nat. Geosci* 2, 718–724. doi:10.1038/ngeo636

Su, X., Yao, L., Wu, W., Meng, G., Su, L., Xiong, R., et al. (2018). Crustal Deformation on the Northeastern Margin of the Tibetan Plateau from Continuous GPS Observations. *Remote Sensing* 11 (1), 34. doi:10.3390/rs11010034

Tapponnier, P. (2001). Oblique Stepwise Rise and Growth of the Tibet Plateau. *Science* 294 (5547), 1671–1677. doi:10.1126/science.105978

Tapponnier, P., Peltzer, G., Dain, A. Y. L., Armijo, R., and Cobbold, P. (1982). Propagating Extrusion Tectonics in Asia: New Insights from Simple Experiments with Plasticine. *Geology* 10 (12), 611–616. doi:10.1130/0091-7613(1982)10<611:PETIAN>2.0.CO;2

Tian, Q. J., Ding, G. Y., and Shen, X. H. (2002). Pull-apart Basins and the Total Lateral Displacement along the Haiyuan Fault Zone in Cenozoic. *Earth Res. China* 17 (2), 167–175. (in Chinese with English abstract). doi:10.3969/j.issn.1001-4683.2001.02.007

Wang, H., Liu, M., Cao, J., Shen, X., and Zhang, G. (2011). Slip Rates and Seismic Moment Deficits on Major Active Faults in mainland China. *J. Geophys. Res.* 116 (B2), B02405. doi:10.1029/2010JB007821

Wang, M., and Shen, Z. K. (2020). Present-Day Crustal Deformation of Continental China Derived from GPS and its Tectonic Implications. *J. Geophys. Res. Solid Earth* 125 (2), e2019JB018774. doi:10.1029/2019JB018774

Wang, Z., Fu, G., and She, Y. (2018). Crustal Density Structure, Lithosphere Flexure Mechanism, and Isostatic State throughout the Qinling Orogen Revealed by *In Situ* Dense Gravity Observations. *J. Geophys. Res. Solid Earth* 123 (11), 10026–10039. doi:10.1029/2018JB016117

Wessel, P., and Smith, W. F. H (1998). New, improved version of Generic Mapping Tools released, EOS Trans. *AGU* 79 (47), 579. doi:10.1029/98EO00426

Yang, Y., Ritzwoller, M. H., Zheng, Y., Shen, W., Levshin, A. L., and Xie, Z. (2012). A Synoptic View of the Distribution and Connectivity of the Mid-crustal Low Velocity Zone beneath Tibet. *J. Geophys. Res.* 117 (B4), a–n. doi:10.1029/2011jb008810

Yao, W., Liu-Zeng, J., Oskin, M. E., Wang, W., Li, Z., Prush, V., et al. (2019). Reevaluation of the Late Pleistocene Slip Rate of the Haiyuan Fault Near Songshan, Gansu Province, China. *J. Geophys. Res. Solid Earth* 124 (5), 5217–5240. doi:10.1029/2018JB016907

Ye, Z., Li, J., Gao, R., Song, X., Li, Q., Li, Y., et al. (2017). Crustal and Uppermost Mantle Structure across the Tibet-Qinling Transition Zone in NE Tibet: Implications for Material Extrusion beneath the Tibetan Plateau. *Geophys. Res. Lett.* 44 (20), 316–410. doi:10.1002/2017GL075141

Yu, Y., and Chen, Y. J. (2016). Seismic Anisotropy beneath the Southern Ordos Block and the Qinling-Dabie Orogen, China: Eastward Tibetan Asthenospheric Flow Around the Southern Ordos. *Earth Planet. Sci. Lett.* 455, 1–6. doi:10.1016/j.epsl.2016.08.026

Yuan, D. Y., Ge, W. P., Chen, Z. W., Li, C. Y., Wang, Z. C., Zhang, H. P., et al. (2013). The Growth of Northeastern Tibet and its Relevance to Large-scale continental Geodynamics: A Review of Recent Studies. *Tectonics* 32 (5), 1358–1370. doi:10.1002/tect.20081

Yuan, D. Y., Zhang, P. Z., Liu, B. C., Gan, W. J., Mao, F. Y., Wang, Z. C., et al. (2004). Geometrical Imagery and Tectonic Transformation of Late Quaternary Active Tectonics in Northwestern Margin of Qinghai- Xizang Plateau. *Acta Geol. Sin* 78 (2), 270–278. (in Chinese with English abstract).

Zhang, P. Z., Shen, Z., Wang, M., Gan, W., Bürgmann, R., Molnar, P., et al. (2004). Continuous Deformation of the Tibetan Plateau from Global Positioning System Data. *Geol.* 32 (9), 809. doi:10.1130/G20554.1

Zheng, J. P., Griffin, W. L., Sun, M., O'Reilly, S. Y., Zhang, H. F., Zhou, H. W., et al. (2010). Tectonic Affinity of the West Qinling Terrane (central China): North China or Yangtze?: TECTONIC AFFINITY of the WEST QINLING TERRANE. *Tectonics* 29 (2), na. doi:10.1029/2008TC002428

Zheng, W. J., Zhang, P. Z., He, W. G., Yuan, D. Y., Shao, Y. X., Zheng, D. W., et al. (2013). Transformation of Displacement between Strike-Slip and Crustal Shortening in the Northern Margin of the Tibetan Plateau: Evidence from Decadal GPS Measurements and Late Quaternary Slip Rates on Faults. *Tectonophysics* 584, 267–280. doi:10.1016/j.tecto.2012.01.006

Zheng, W. J., Liu, X. W., Yu, J. X., Yuan, D. Y., Zhang, P. Z., Ge, W. P., et al. (2016). Geometry and Late Pleistocene Slip Rates of the Liangdang-Jiangluo Fault in the Western Qinling Mountains, NW China. *Tectonophysics* 687, 1–13. doi:10.1016/j.tecto.2016.08.021

Zuza, A. V., and Yin, A. (2016). Continental Deformation Accommodated by Non-rigid Passive Bookshelf Faulting: An Example from the Cenozoic Tectonic Development of Northern Tibet. *Tectonophysics* 677-678, 227–240. doi:10.1016/j.tecto.2016.04.007